S. Fernandez, I. Lopetegi, L. Oca, J. Yeregui, E. Garayalde and U. Iraola, "Intuitive Degradation Mode Estimation Tool: ModEst," 2024 Energy Conversion Congress & Expo Europe (ECCE Europe), Darmstadt, Germany, 2024, pp. 1-7.

DOI: https://doi.org/10.1109/ECCEEurope62508.2024.10751868

Intuitive Degradation Mode Estimation Tool: ModEst

Sergio Fernandez
Electronics and Computing Department
Mondragon Unibertsitatea
Hernani, Spain
sergio.fernandez@alumni.mondragon.edu

Iker Lopetegi
Electronics and Computing Department
Mondragon Unibertsitatea
Hernani, Spain
ilopetegui@mondragon.edu

Laura Oca
Electronics and Computing Department
Mondragon Unibertsitatea
Hernani, Spain
lauraoca@mondragon.edu

Josu Yeregui
Electronics and Computing Department
Mondragon Unibertsitatea
Hernani, Spain
jyeregui@mondragon.edu

Erik Garayalde
Electronics and Computing Department
Mondragon Unibertsitatea
Hernani, Spain
egarayalde@mondragon.edu

Unai Iraola
Electronics and Computing Department
Mondragon Unibertsitatea
Hernani, Spain
uiraola@mondragon.edu

***Abstract*—Battery ageing is one of the main concerns in most battery applications. To reduce this degradation rate, it is key to understand how batteries age. However, the diagnosis of battery ageing is very challenging due to the little information that can be obtained without disassembling the battery cells. This paper presents a tool for battery degradation diagnosis. By a multi-objective optimisation algorithm, the tool estimates three degradation modes that lead to capacity fade: the loss of active material (LAM) of each electrode, and the loss of lithium inventory (LLI). The stepwise methodology tool is exposed and proved on three different degradation scenarios and battery cell chemistries. Two of the scenarios were simulated using a physics-based model (PBM), and the other scenario was obtained from an experimental degradation study. The results demonstrate accuracy and robustness of the tool while offering great simplicity and intuitiveness compared to other tools reported in the literature.**

***Index Terms*—Degradation modes, battery ageing diagnosis, open-circuit-potential OCP, differential voltage analysis.**

I. Introduction

Battery systems, particularly those integrating Lithium-ion cells, are deeply reliant on their performance and degradation attributes, which are subject to influence from variables such as usage patterns and environmental conditions [1]. Accurate diagnosis of battery degradation holds paramount importance for the efficient management of energy across diverse power sources, thereby facilitating informed decisions concerning safe utilisation and potential re-usability [2]. This underscores the critical need for conducting comprehensive health assessments during their useful life.

The estimation of lithium-ion battery degradation is a challenging research topic due to the complex nature of several degradation mechanisms that can occur inside battery cells [3]. Most common methods for estimating degradation are the capacity fade analysis and internal resistance measurement [4]. The state-of-health (SOH) of a battery or cell is usually calculated as the ratio of the actual cell capacity (measured under the specified protocol by the manufacturer) and the nominal cell capacity, which represents the fraction of the actual battery capacity against its nominal value. However, this capacity value is not completely representative of the actual health of the components of the battery. Different studies showed that capacity fade and internal resistance increase, which are the most monitored effects, may only be the tip of the iceberg of the degradation matrix [4], [5], since they may not show the actual amount of ageing that the battery has suffered.

Several degradation mechanisms could happen simultaneously during degradation of battery cells [3], but all these mechanisms can be grouped into three main degradation modes depending on how the mechanisms affect the thermodynamic behavior of the cell [5], [6]: LAM of both electrodes and LLI. Various authors have classified numerous degradation mechanisms using degradation modes [3], [6], [7]. The estimation of specific degradation mechanisms would be extremely challenging, if not impossible, using current and voltage measurements. However, since these degradation modes directly affect the open-circuit voltage (OCV) of the cell [5], [6], the estimation of these modes is more tractable, and could give more insight about battery aging than just a capacity loss value.

In response to this, a tool that provides further information on battery degradation modes is needed. Different tools have been presented in the literature. Birkl *et al*. [6] conducted degradation mode estimation by means of OCV fitting. On the other hand, Wu *et al*. [8] presented a tool to estimate degradation modes by assigning the observed incremental capacity (dQ/dV) and differential voltage (dV/dQ) peaks to each of the electrodes. Both tools present precise results in their own, but may miss in each other considerations. Also, they lack on intuitiveness, ease of use and robustness, as they do not present results for different Li-ion chemistries.

Both authors presented above exhibit the fact that the OCV is the combination of the open-circuit-potential (OCP) of the

positive and negative electrodes within their stoichiometry limits between 100 % and 0 % SOC. The stoichiometry is defined as the ratio between the lithium concentration intercalated in an active material particle, and the maximum theoretical lithium concentration that the material can embrace. Figure 1 shows the relation between the OCV of the cell and the OCPs of the electrodes. As shown, the OCV/capacity relation of the cell comes from the combination of the OCPs of the electrodes. When batteries age, the relation between OCPs change, since the electrodes can lose capacity due to LAM and there might occur a shift between both electrodes due to LLI [5], [6].

The OCP refers to the active material potential considering a Li/Li$^+$ reference electrode when the current flowing is null. OCV varies as a function of different conditions, but mainly as a function of the state-of-charge (SOC). On the other hand, OCP is dependant on the state-of-lithiation (SOL) of the electrode. When charging a battery cell, positive electrode is delithiated while negative electrode is lithiated and vice versa for discharging. When a battery cell is manufactured, the capacity of the electrodes is larger than the cell capacity itself, meaning that the SOC window is placed somewhere inside the SOL window of the electrodes.

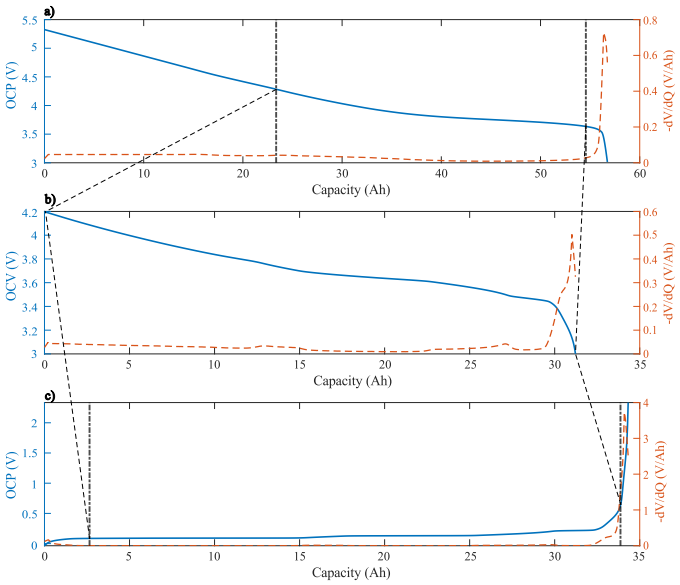

Fig. 1. OCV-OCP relation of a NMC cell: a) positive electrode OCP and differential voltage curve, b) cell OCV and differential voltage curve, c) negative electrode OCP and differential voltage curve

Hence, the OCV can be calculated as:

$$OCV = OCP^p(\theta^p) - OCP^n(\theta^n)\ . \tag{1}$$

Where OCP^p and OCP^n stand for positive and negative electrode potentials at open-circuit. θ^p and θ^n refer to the stoichiometry of each electrode.

In this paper, a tool capable of estimating Li-ion battery degradation modes is presented. The core of the tool is a multi-objective optimisation algorithm. It considers both OCV error minimisation and differential voltage (dV/dQ) error minimisation between estimated and real curves, finding the optimal point in the Pareto front. The main strengths of the developed tool are:

- Intuitiveness and ease of use.
- Precision.
- Robustness, as it works well in different cell chemistries.
- Low computational cost.

The paper is organised as follows. In Section II, the methodology of the developed tool is explained. The results are illustrated and discussed in Section III. Finally, the main conclusions of the study are presented in Section IV.

II. Tool Description

The developed tool performs a multi-objective optimisation using a genetic algorithm (GA). Genetic algorithm is an heuristic approach that seeks the minimisation of the objective function by evolving a population of randomly generated individuals through an iterative process. Hence, the algorithm can be iterated continuously until a sufficiently accurate value is obtained or error threshold is reached. First, the tool obtains the stoichiometry values at 100 % and 0 % SOC for the beginning-of-life (BOL) OCV. Later, the constraints for the optimisation of the aged cell are calculated based on the BOL optimisation results. Then, the optimisation for the aged cell is computed, so, two optimisation processes are concatenated. Finally, from the results obtained at both optimisation processes the degradation modes are calculated.

The inputs for the tool are the following:

- BOL OCV containing voltage, capacity and SOC data.
- BOL OCP containing potential, capacity and SOL data.
- Scaling information: Electrode size data or reconstructed cell capacity.
- Aged OCV containing voltage, capacity and SOC data.

The outputs of the tool are the following:

- 100 % and 0 % SOC stoichiometries of both electrodes at BOL and for the aged cell.
- Loss-of-active-material (LAM) of each electrode.
- Loss-of-lithium-inventory (LLI).

A. Half-cell scaling

As mentioned above, the cell OCV is obtained by subtracting the negative electrode OCP to the positive electrode OCP within their stoichiometry values between 100 % and 0% SOC, as shown in equation (1). The OCV curves can be obtained by applying techniques as quasi-static voltage measurement or voltage relaxation in the full commercial or prototyped cell. However, the obtention of the OCP of each electrode is not as immediate as obtaining the OCV. To obtain the OCPs of the electrodes, reconstructed cells are usually built using a small portion of the electrode. An example of this methodology is explained in [10]. Different experimental approaches exist, being the most commonly used the coin half-cell (facing up the electrode to a lithium metal foil) [10] and the three-electrode cell (facing up the electrode to a lithium metal foil and including a lithium metal reference

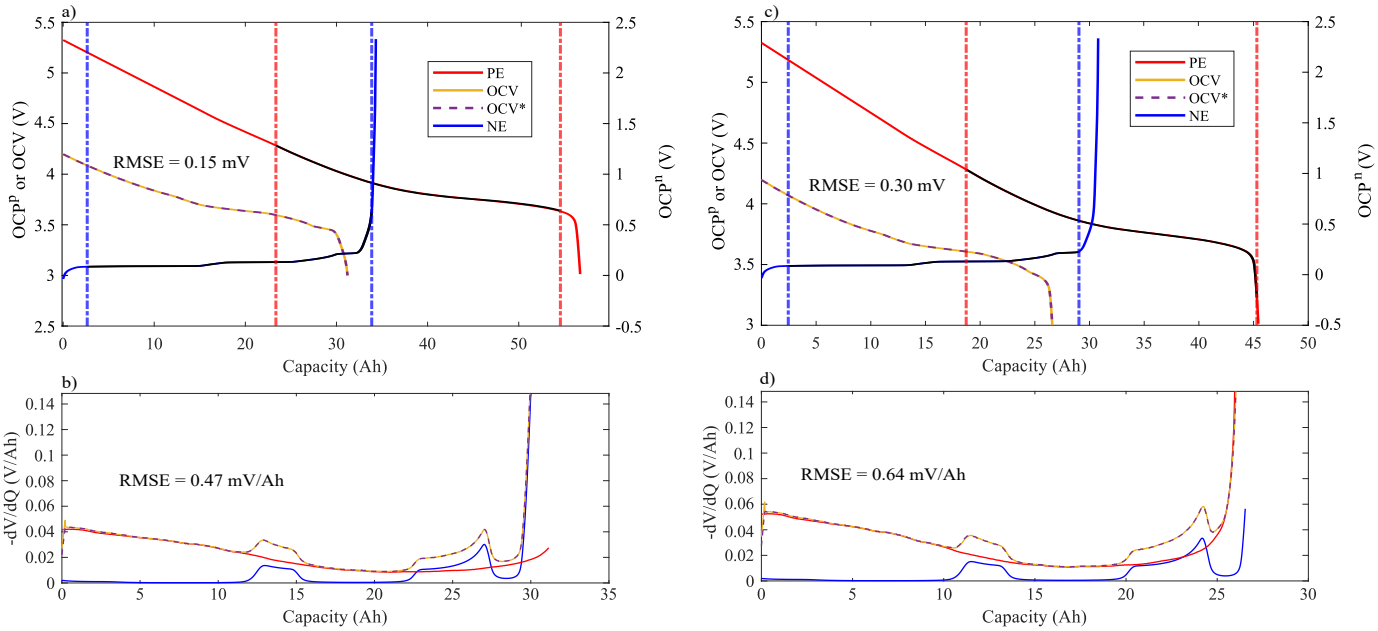

Fig. 2. NMC cell [9] results: BOL optimisation a) OCV and b) dV/dQ fitting results, aged cell optimisation c) OCV and d) dV/dQ fitting results.

electrode) [11]. Preferably, the applied cycling protocol (quasi-static voltage measurement or voltage relaxation) should be the same as in the full cell (scaling the analysed cell capacity). Once the OCPs of the coin cells are acquired, they have to be scaled to the original cell dimensions, increasing its capacity as in Figure 3. The tool admits two ways of scaling techniques chosen by the user: by capacity or by electrochemically active area.

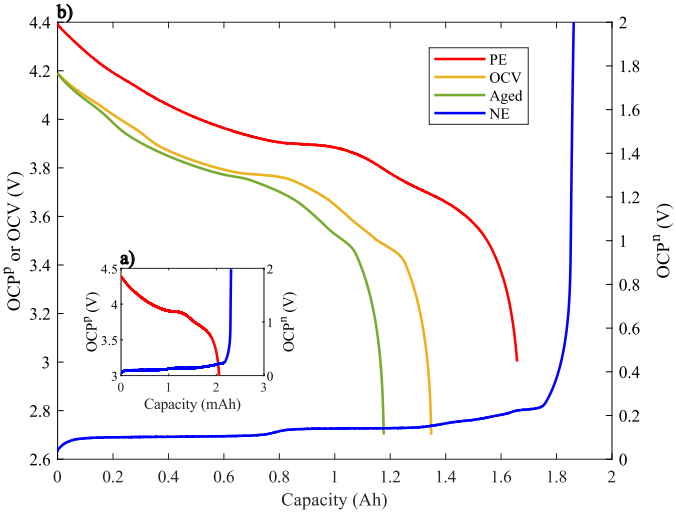

Fig. 3. Kokam, reference SLPB554374H coin-cell scaling [10]: a) reconstructed electrode curves, b) OCP and OCV curves at full-size scale

The first method uses the reconstructed cell level electrode area and the full-size cell electrode area to obtain the scaling factor as

$$Q^r = Q^r_{rec}\frac{A^r}{A^r_{rec}}, \tag{2}$$

where Q^r stands for the electrode capacity in the commercial cell scale, Q^r_{rec} for the electrode capacity in the coin cell scale, and A^r and A^r_{rec} for the electrode area in the commercial cell and the reconstructed cell, respectively. To apply this method, the thicknesses of the electrodes need to be the same in both commercial cell and reconstructed cell and their dimensions need to be measured precisely. As the reconstructed electrodes are the same, the thickness criteria is fulfilled. The calculation of the electrochemically active area on both, reconstructed and commercial cell, is not straightforward (although it should). In reconstructed small cells, the electrode positioning when producing a coin or three-electrode cell might affect this area. Also, in big commercial or prototype cells the quantification or this area should be very precise to obtain accurate scaling results.

The second method requires an extra full reconstructed cell (in addition to half-cells) to perform the scaling. When using this full reconstructed cell, having the same electrochemically active area of each half-cell, the scaling rate is more direct (and considers other factors through the reconstruction process, such as the use of different separator or electrolyte, that the first method do not). This method compares reconstructed full cell capacity and full-size cell capacity to obtain the electrode capacity in the full-size cell scale as

$$Q^r = Q^r_{rec}\frac{Q}{Q_{rec}}, \tag{3}$$

where Q is the full-size cell capacity and Q_{rec} is the reconstructed cell capacity. Both methods are consistent and should present very similar results.

B. Optimisation algorithm

The next step of the optimisation process is the core of the developed tool. To estimate the degradation modes, 100 % and

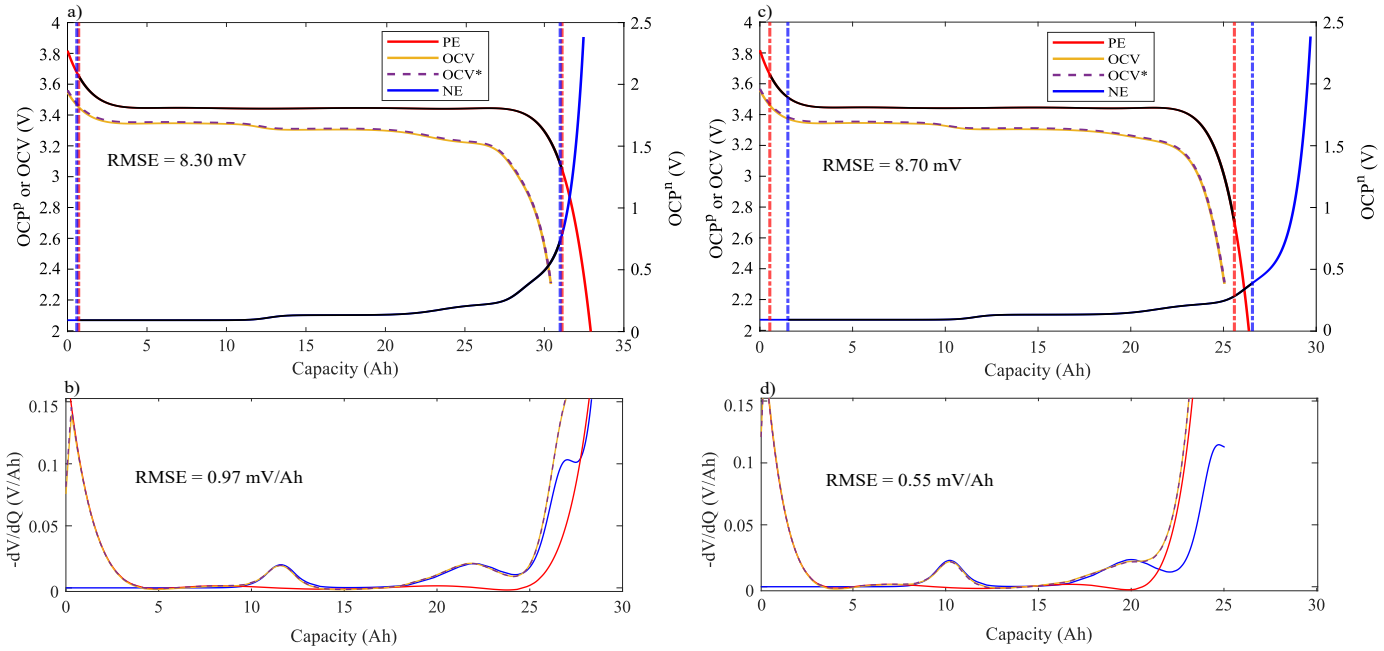

Fig. 4. LFP cell [12] [13] results: BOL optimisation a) OCV and b) dV/dQ fitting results, aged cell optimisation c) OCV and d) dV/dQ fitting results.

0 % SOC stoichiometry values at BOL and for the aged cell are needed. The optimisation procedure for both conditions is the same. The parameters to optimise are:

- Upper stoichiometry capacity value $[Q^n(\theta^n_{100}), [Q^p(\theta^p_{100})]$.
- Electrode capacity variation coefficients $[\alpha^n, \alpha^p]$

The optimisation process is limited by physical constraints. Upper stoichiometry capacity value cannot be lower than 0 nor a capacity value that makes the remaining capacity in the electrode between the 100 % and 0 % SOC stoichiometries to be lower than the cell capacity. Electrode capacity coefficient cannot make the electrode capacity to be lower than the actual cell capacity and can go as high as the total electrode capacity. Therefore, the optimisation global constraints at BOL are calculated as:

$$0 \leq Q^r_{BOL}(\theta^r_{100}) \leq Q^r - Q \ , \tag{4}$$

$$\frac{Q}{Q^r} \leq \alpha^r_{BOL} \leq 1 \ . \tag{5}$$

As stated above, aged optimisation maximum constraints may be different to BOL constraints, as they depend on the result of BOL optimisation. Upper stoichiometry capacity value and maximum capacity coefficient constraints for the aged cell optimisation are redefined as follows:

$$0 \leq Q^r_a(\theta^r_{100}) \leq Q^r_{BOL} - Q \tag{6}$$

$$\frac{Q}{Q^r} \leq \alpha^r_a \leq \frac{Q}{Q^r_{BOL}} \tag{7}$$

To keep the capacity of the electrodes above the capacity of the cell, a nonlinear inequality constraint is added in both optimisations as

$$\alpha^r Q^r - Q^r(\theta^r_{100}) \geq Q \ . \tag{8}$$

The lower stoichiometry capacity value is obtained as follows either for the BOL or for the aged cell:

$$Q^r(\theta^r_0) = Q^r(\theta^r_{100}) + Q \ . \tag{9}$$

The OCP of each electrode is calculated as:

$$OCP^r(\theta^r) = OCP^r(Q^r(\theta^r_{100}), Q^r(\theta^r_0)) \tag{10}$$

From the calculated OCP curves, OCV is calculated as in equation 1, and the differential voltage is calculated as:

$$\frac{dV}{dQ} = \frac{dOCV}{dQ}. \tag{11}$$

The cost functions to minimise are the OCV and the dV/dQ root mean square errors, which emphasises big errors and is consistent with average values.

$$J_1 = \sqrt{\frac{1}{n}\sum_{i=1}^{n}(OCV_i - OCV_i^*)^2} \tag{12}$$

$$J_2 = \sqrt{\frac{1}{n}\sum_{i=1}^{n}\left(\frac{dV}{dQ}_i - \frac{dV}{dQ}_i^*\right)^2} \tag{13}$$

An example of the fitting evolution during the execution of the tool can be seen in the Appendix.

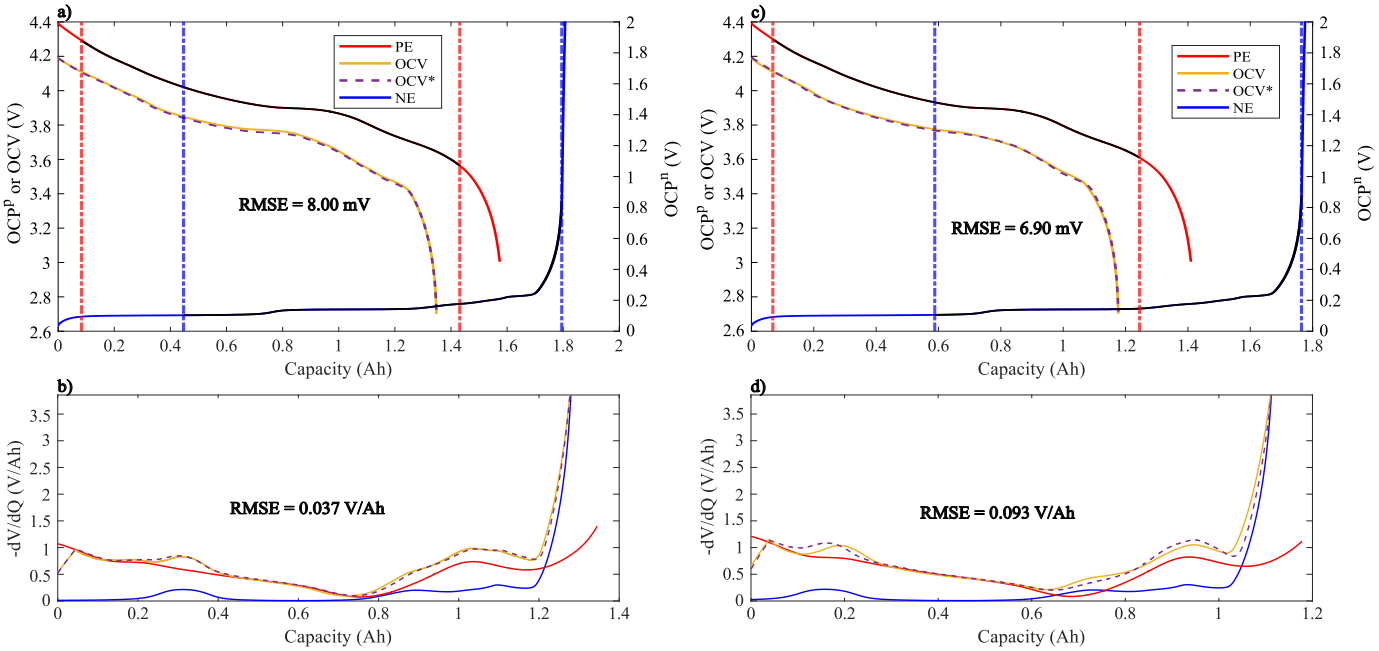

Fig. 5. Kokam SLPB554374H results: BOL optimisation a) OCV and b) dV/dQ fitting results, aged cell optimisation c) OCV and d) dV/dQ fitting results.

C. Degradation modes estimation

The LAM of an electrode is given by:

$$LAM^r = \left(1 - \frac{Q_a^r}{Q_{BOL}^r}\right) \times 100 \tag{14}$$

To calculate the LLI, first, the total amount of intercalated lithium in the cell at any SOC was as

$$n_{Li} = \frac{3600}{F}\left(z^p Q^p + z^n Q^n\right), \tag{15}$$

where z^n and z^p stand for the SOL values for the negative and positive electrodes that can be chosen from the entire SOC range (both from the same SOC). In our case, we have chosen to take the 100 % SOC values. F is the Faraday constant. Then, the LLI can be calculated as

$$LLI = \left(1 - \frac{n_{Li}^a}{n_{Li}^{BOL}}\right), \times 100 \tag{16}$$

where n_{Li}^a is the aged lithium inventory, and n_{Li}^{BOL} is the lithium amount in the cell at BOL.

III. Validation

To validate the estimates of the tool, in this section, we present the results obtained at different degradation scenarios for (a) simulation and (b) experimental data. To make the validation process as faithful as possible, different battery chemistries were evaluated, since different OCP curves can make the estimation process more or less difficult [14]. The results show the OCV and differential voltage fitting accuracy, the stoichiometry of the electrodes, and the estimation of the degradation modes.

A. Simulation degradation scenarios

Two different cells were used for the simulation validation process. On the one hand, data from a high-power 28 Ah NMC/graphite cell was acquired from [9]. On the other hand, a LFP/graphite-Si cell was simulated to include a more challenging scenario in the validation process. It is well known that flat OCP curves lead to lower observability [14], and thus, an LFP/graphite cell should be one of the most difficult cells for degradation mode estimation. The OCP data for the LFP electrode was obtained from [12], and the graphite-Si electrode data from [13]. NMC technology presents higher OCV observability than LFP technology due to former's steeper OCV behaviour. Therefore, in terms of OCV and differential voltage curve fitting, higher accuracy is expected for the NMC cell. The simulated OCV data was obtained using the single-particle model with electrolyte dynamics (SPMe) presented in [15], and the aged conditions were achieved by applying the LAM and LLI values in the parameters of the SPMe as in [16]. After adjusting the parameters, OCV simulations were carried out to obtain the aged OCV data. Visual representation of the curve fitting can be seen in Figure 2 and Figure 4. As can be observed, the algorithm is able to correctly fit the OCVs, with low root mean square (RMS) errors, as well as the differential voltage curves in both cases. The estimated degradation modes can be seen in Table I. As shown, the tool is able to estimate the three degradation modes with high accuracy in both simulation degradation cases. For the NMC cell reltive differences of 2 % for LAM^n, 0 % for LAM^p and 0.2 for % LLI have been obtained. In the case of the LFP cell, differences of 2.6 % for LAM^n, 0.7 for % LAM^p and 0.75 for % LLI.

TABLE I
SIMULATION DEGRADATION MODES ESTIMATION

		LAM^n	LAM^p	LLI
NMC	Estimated	9.80 %	20.00 %	14.51 %
	Expected	10.00 %	20.00 %	14.48 %
LFP	Estimated	9.74 %	19.86 %	12.09 %
	Expected	10.00 %	20.00 %	12.00 %

B. Experimental degradation scenario

A 1.25Ah high-power cell (Kokam, reference SLPB554374H) was used for this scenario. The negative active material is composed of graphite, and the positive active material is a mixture of Lithium Cobalt Dioxide ($LiCoO_2$) and Lithium Nickel Cobalt Oxide ($LiNiCoO_2$). The methodology for coin cell reconstruction, scaling, and OCP curves of the materials was obtained from [10]. The cell OCV was experimentally tested at BOL and EOL. For this study, 1C-1C symmetric cycles at 25 ºC were employed. The OCP curves scaling and OCV tests at both life instants are shown in Figure 3. The OCV and differential voltage fitting results are shown in Figure 5 and the estimated degradation modes are: 0.5 % LAM^n, 10.80 % LAM^p and 11.66 % LLI. As can be seen in Figure 5, the fitting of the OCV is accurate, and the peaks of the OCPs are well aligned with the OCV peaks, which gives confidence to the degradation mode estimates.

IV. CONCLUSIONS

In this paper, a novel tool for the diagnosis of battery degradation was presented. The tool is capable of estimating the loss of active material and loss of lithium inventory among different cell chemistries and degradation levels. The tool has been first validated in simulated scenarios and has then proven its effectiveness in experimental working conditions. Relative differences below 2.5 % have been obtained for the degradation modes estimation and curve fitting RMS values below 8.7 mV even for the LFP cell, where the estimation is more challenging as previously mentioned.

Experimental data from a previously aged LCO/NCA-graphite cell was used to estimate the degradation modes, obtaining that the negative electrode has suffered a LAM of 0.5 %, the positive electrode of 10.80 %, and the amount of lithium in the cell has decreased 11.66 %. The differential voltage peaks were well aligned and the RMS error of the OCV was below 7 mV, suggesting that the degradation mode estimates are reliable.

All in all, the tool can be used in a wide range of applications including lithium-ion batteries, accurately diagnosing the degradation during their operating lifetime. In addition, the tool can be used for electrode balancing purposes, which is applicable in several modelling and characterisation applications to determine the lithiation ranges of the electrodes.

REFERENCES

[1] P. P. Mishra, A. Latif, M. Emmanuel, Y. Shi, K. McKenna, K. Smith, and A. Nagarajan, "Analysis of degradation in residential battery energy storage systems for rate-based use-cases," *Applied Energy*, vol. 264, p. 114632, 2020.

[2] Y. Zhao, O. Pohl, A. I. Bhatt, G. E. Collis, P. J. Mahon, T. Rüther, and A. F. Hollenkamp, "A review on battery market trends, second-life reuse, and recycling," *Sustainable Chemistry*, vol. 2, no. 1, pp. 167–205, 2021.

[3] J. S. Edge, S. O'Kane, R. Prosser, N. D. Kirkaldy, A. N. Patel, A. Hales, A. Ghosh, W. Ai, J. Chen, J. Yang, S. Li, M.-C. Pang, L. Bravo Diaz, A. Tomaszewska, M. W. Marzook, K. N. Radhakrishnan, H. Wang, Y. Patel, B. Wu, and G. J. Offer, "Lithium ion battery degradation: what you need to know," *Physical Chemistry Chemical Physics*, vol. 23, no. 14, pp. 8200–8221, 2021.

[4] Y. Liu, C. Liu, Y. Liu, F. Sun, J. Qiao, and T. Xu, "Review on degradation mechanism and health state estimation methods of lithium-ion batteries," *Journal of Traffic and Transportation Engineering (English Edition)*, 2023.

[5] M. Dubarry, C. Truchot, and B. Y. Liaw, "Synthesize battery degradation modes via a diagnostic and prognostic model," *Journal of power sources*, vol. 219, pp. 204–216, 2012.

[6] C. R. Birkl, M. R. Roberts, E. McTurk, P. G. Bruce, and D. A. Howey, "Degradation diagnostics for lithium ion cells," *Journal of Power Sources*, vol. 341, pp. 373–386, 2017.

[7] J. Vetter, P. Novák, M. R. Wagner, C. Veit, K. C. Möller, J. O. Besenhard, M. Winter, M. Wohlfahrt-Mehrens, C. Vogler, and A. Hammouche, "Ageing mechanisms in lithium-ion batteries," *Journal of Power Sources*, vol. 147, pp. 269–281, 2005.

[8] J. Chen, M. N. Marlow, Q. Jiang, and B. Wu, "Peak-tracking method to quantify degradation modes in lithium-ion batteries via differential voltage and incremental capacity," *Journal of Energy Storage*, vol. 45, p. 103669, 2022.

[9] J. Schmalstieg, C. Rahe, M. Ecker, and D. U. Sauer, "Full cell parameterization of a high-power lithium-ion battery for a physico-chemical model: Part i. physical and electrochemical parameters," *Journal of The Electrochemical Society*, vol. 165, no. 16, pp. A3799–A3810, 2018.

[10] L. Oca, E. Miguel, E. Agirrezabala, A. Herran, E. Gucciardi, L. Otaegui, E. Bekaert, A. Villaverde, and U. Iraola, "Physico-chemical parameter measurement and model response evaluation for a pseudo-two-dimensional model of a commercial lithium-ion battery," *Electrochimica Acta*, vol. 382, p. 138287, 2021.

[11] J. Costard, M. Ender, M. Weiss, and E. Ivers-Tiffée, "Three-electrode setups for lithium-ion batteries," *Journal of The Electrochemical Society*, vol. 164, no. 2, p. A80, 2016.

[12] E. Prada, D. Di Domenico, Y. Creff, J. Bernard, V. Sauvant-Moynot, and F. Huet, "Simplified electrochemical and thermal model of lifepo4-graphite li-ion batteries for fast charge applications," *Journal of The Electrochemical Society*, vol. 159, no. 9, p. A1508, 2012.

[13] C.-H. Chen, F. B. Planella, K. O'regan, D. Gastol, W. D. Widanage, and E. Kendrick, "Development of experimental techniques for parameterization of multi-scale lithium-ion battery models," *Journal of The Electrochemical Society*, vol. 167, no. 8, p. 080534, 2020.

[14] I. Lopetegi, G. L. Plett, M. S. Trimboli, A. Kawakita de Souza, L. Oca, E. Miguel, and U. Iraola, "A New Battery SOC/SOH/eSOH Estimation Method Using a PBM and Interconnected SPKFs: Part I. SOC and Internal Variable Estimation," *Journal of The Electrochemical Society*, 2024. [Online]. Available: http://iopscience.iop.org/article/10.1149/1945-7111/ad30d4

[15] I. Lopetegi, G. L. Plett, M. S. Trimboli, J. Yeregui, L. Oca, C. Rojas, E. Miguel, and U. Iraola, "Lithium-ion battery aging prediction with electrochemical models: P2d vs spme," in *2023 IEEE Vehicle Power and Propulsion Conference (VPPC)*. IEEE, 2023, pp. 1–7.

[16] I. Lopetegi, G. L. Plett, M. S. Trimboli, L. Oca, E. Miguel, and U. Iraola, "A New Battery SOC/SOH/eSOH Estimation Method Using a PBM and Interconnected SPKFs: Part II. SOH and eSOH Estimation," *Journal of The Electrochemical Society*, 2024. [Online]. Available: http://iopscience.iop.org/article/10.1149/1945-7111/ad30d5

APPENDIX

As stated in Section II-B, the next Figures 6 and 7 illustrate the progression of the optimisation algorithm for the 1.25Ah high-power cell (Kokam, reference SLPB554374H) for the BOL OCV curve. Figure 6 specifically presents the initial Pareto front, showcasing the associated scores distribution and the population values.

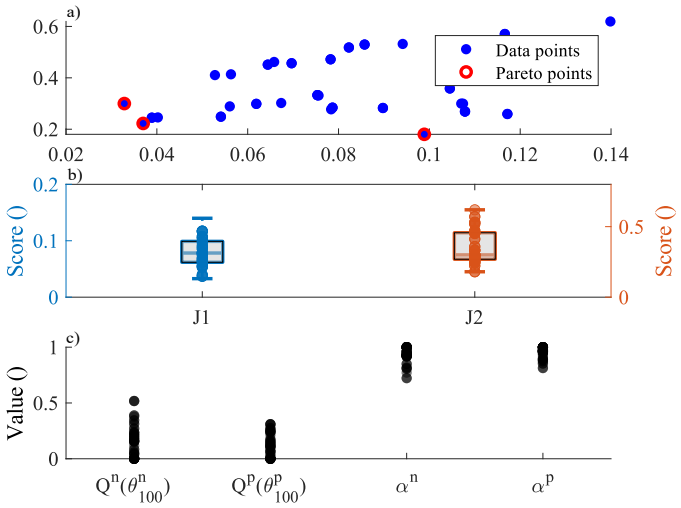

Fig. 6. Initial population scores and Pareto front (a), cost function scores distribution (b) and individual values dispersion (c) for Kokam, reference SLPB554374H, cell BOL optimization.

Figure 7 displays the results for the final population, demonstrating its convergence towards a global minimum.

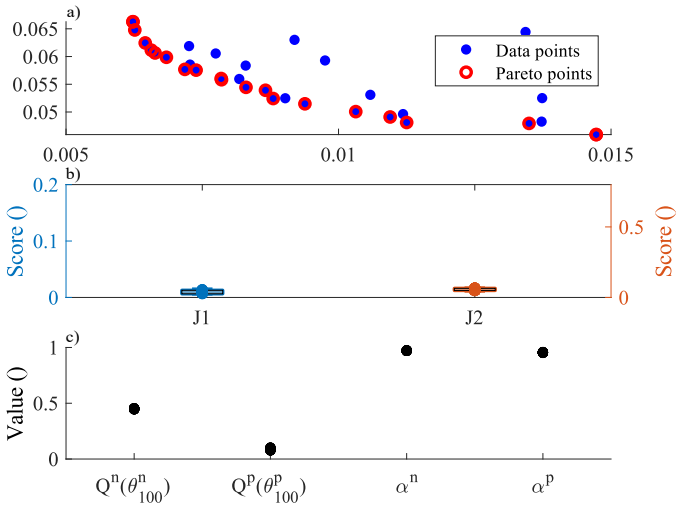

Fig. 7. Last population scores and Pareto front (a), cost function scores distribution (b) and individual values dispersion (c) for Kokam, reference SLPB554374H, cell BOL optimization.